BMC Plant Biology

https://doi.org/10.1186/s12870-026-09066-9

Article in Press

Chickpea chitinases responsive to Helicoverpa herbivory and phytohormone signaling: genome-wide identification, field expression profiling, and structure-guided prioritization

Received: 5 April 2026

Accepted: 20 May 2026

Published online: 04 June 2026

Cite this article as: Konda A.K., Annapragada H., G.K. S. *et al.* Chickpea chitinases responsive to Helicoverpa herbivory and phytohormone signaling: genome-wide identification, field expression profiling, and structure-guided prioritization. *BMC Plant Biol* (2026). https://doi.org/10.1186/s12870-026-09066-9

Aravind Kumar Konda, Harika Annapragada, Sujayanand G.K., Pooja Singh, Bhoopal Bhuvanachandra, Hariharan V. Chinnasamy, Girish Prasad Dixit, Kapuganti Jagadis Gupta & Saravanan Matheshwaran

Chickpea chitinases responsive to Helicoverpa herbivory and phytohormone signaling: genome-wide identification, field expression profiling, and structure-guided prioritization

Aravind Kumar Konda[1]*, Harika Annaparagada[1], Sujayanand G.K.[1], Pooja Singh[2], Bhoopal Bhuvanachandra[3], Hariharan V Chinnasamy[4], Girish Prasad Dixit[1], Kapuganti Jagadis Gupta[2], Saravanan Matheshwaran[4]*

1 ICAR-Indian Institute of Pulses Research, Kanpur, Uttar Pradesh 208024, India

2 BRIC-National Institute of Plant Genome Research, Aruna Asaf Ali Marg, New Delhi 110067, India

3 University of Hyderabad, Hyderabad, Telangana 500046, India

4 Indian Institute of Technology Kanpur, Kanpur, Uttar Pradesh 208016, India

Correspondence: Aravind Kumar Konda (arvind.konda@icar.org.in; aravindbio@gmail.com) and

Co-correspondence: Saravanan Matheswaran (saran@iitk.ac.in; saran240478@gmail.com)

Abstract

Background: Chitinases can contribute to plant defence against fungal pathogens and insect herbivores, but their family organization, inducible deployment, and putative ligand-recognition behaviour remain poorly resolved in chickpea. We combined genome-wide identification, field expression profiling under controlled *Helicoverpa armigera* infestation, hormone treatments, and structure-guided comparison of representative proteins to prioritize defence-associated chickpea chitinases.

Results: We identified 28 chickpea chitinase loci (Car_Chits), comprising 22 glycosyl hydrolase family 18 (GH18) genes and 6 GH19 genes. Local duplication, especially tandem duplication within GH18, was the main contributor to family expansion, and interpretable duplicate pairs were retained mainly under purifying selection. Promoter scans indicated broad enrichment of defence- and hormone-associated cis-elements. Field quantitative real-time PCR (qRT-PCR) profiling of 11 candidate genes in field-grown plants subjected to controlled *H. armigera* infestation and hormone treatments showed treatment-specific temporal regulation. Car_Chit-4 (GH19) was strongly induced by salicylic acid (7.81-fold at 0.5 h; $q < 0.05$) but transiently repressed shortly after *H. armigera* feeding (0.15-fold at 0.5 h; $q = 0.030$). Car_Chit-19 (GH18) was the clearest herbivory-responsive gene, with late induction at 8 h (1.62-fold; $q = 0.050$) and 48 h (1.85-fold; $q = 0.050$). Jasmonic acid caused broad early repression across several genes, followed by delayed induction of Car_Chit-4 at 24 h. Seven Car_Chit-$(GlcNAc)_4$ complexes were modelled, docked, and simulated for 100 ns. GH18 proteins generally showed more favourable predicted MM-PBSA binding energies than GH19 proteins, but the structural metrics were interpreted as relative ligand-recognition indicators rather than direct evidence of anti-herbivore function. Car_Chit-17 had the most favourable predicted binding energy ($\Delta G_{bind} = -18.51 \pm 6.75$ kcal/mol), whereas Car_Chit-14 and Car_Chit-27 retained the most stable ligand poses and Car_Chit-19 displayed the most stable protein scaffold.

Conclusions: Chickpea chitinases show differentiated temporal responses to herbivory and hormone signalling. The study supports a working model in which GH19 Car_Chit-4 marks a rapid salicylic-acid-responsive arm, whereas GH18 Car_Chit-19 marks a delayed herbivory-responsive arm. A tiered prioritization framework separates expression-deployed candidates from structure-guided biochemical

candidates, explaining why different genes emerge from qRT-PCR and molecular modelling analyses. The structural analyses provide complementary prioritization of Car_Chit-17, Car_Chit-14, and Car_Chit-27 for biochemical characterization. Together, these results provide a resource for dissecting chitinase-mediated defence in chickpea and for selecting candidates for functional validation.

Keywords: *Cicer arietinum*; *Helicoverpa armigera*; chitinase; jasmonic acid; salicylic acid; molecular dynamics; MM-PBSA.

Background

Herbivorous insects remain a major constraint on crop productivity, with *Helicoverpa armigera* ranking among the most destructive chewing pests of grain legumes worldwide [1–4]. In chickpea, severe infestations can cause extensive pod and foliage damage, leading to significant economic losses for farmers [3]. Because repeated insecticide applications carry environmental costs and foster resistance, there is sustained interest in endogenous plant defense genes that could complement or diversify current management strategies [3–4].

Chitinases are attractive candidates in this context because they hydrolyze the β-1,4-linked N-acetyl-D-glucosamine polymer chitin, a key structural component of fungal cell walls and the insect peritrophic matrix [5–12]. Chitinase-mediated disruption of the insect gut barrier has been proposed to enhance direct anti-herbivore activity and to complement other defense strategies, including toxin stacking in transgenic systems [6–7]. Plant chitinases are classified primarily into the GH18 and GH19 families, which differ in sequence, structure, and catalytic architecture [8–9]. Both plant-derived and heterologous chitinases have been associated with improved resistance against lepidopteran pests, although the magnitude and context dependence of these effects vary across species and experimental systems [10–15].

In chickpea, transcriptomic studies of simulated herbivory have revealed rapid activation of hormone-responsive defense pathways [16], and a recent genome-wide analysis identified 27 chitinase genes, primarily in relation to Fusarium stress [17]. However, that inventory was based on an earlier chickpea genome assembly and included two loci on unplaced scaffolds. As a result, the family organization under the updated RefSeq annotation and the identity of chitinases deployed during field herbivory remain insufficiently resolved. This gap is important because mechanical wounding and natural herbivory do not always elicit equivalent molecular responses, particularly when herbivore-derived cues and hormone crosstalk are involved [16,18–22]. Chitinases from pathogenesis-related protein families are also known to respond to salicylic acid (SA), jasmonic acid (JA), and related signaling networks [18–19], raising the possibility that distinct chitinase subsets contribute to different phases of chickpea defense.

We combined genome-wide family analysis, expression profiling in field-grown chickpea under controlled *H. armigera* infestation, hormone time-course experiments, and structure-guided comparisons of representative proteins. Our objectives were to characterize the chickpea chitinase repertoire, determine which members respond to herbivory and SA/JA signalling, and apply docking and molecular dynamics analyses to prioritize candidates for future biochemical and functional validation. Because these approaches measure different biological properties, candidate interpretation was framed as a tiered prioritization scheme rather than as a single overall ranking.

Methods

Identification of chickpea chitinases

Chitinase-encoding genes in chickpea (hereafter *Car_Chits*) were identified by querying the chickpea protein database with consensus profiles for the GH18 (Pfam PF00704) and GH19 (Pfam PF00182) catalytic families. DELTA-BLAST searches were conducted using default parameters [23], and redundant protein hits were collapsed with CD-HIT [24]. Candidate sequences were retained only when conserved chitinase domains were confirmed by SMART and Pfam annotation [25–26]. The final genomic inventory comprised 28 loci; for protein-sequence-based analyses, the identical *Car_Chit-8* and *Car_Chit-9* proteins were represented once, yielding a non-redundant set of 27 sequences.

Chromosomal distribution, duplication analysis, and evolutionary characterization

Genomic coordinates were retrieved from the chickpea RefSeq assembly GCF_000331145.2 and plotted across the eight chromosomes using Circos [27]. Duplication classes were assigned with MCScanX as tandem, proximal, dispersed, singleton, or WGD/segmental [28]. Pairwise nonsynonymous (Ka) and synonymous (Ks) substitution rates were estimated using the Nei–Gojobori method; when this yielded a non-positive Ks estimate, maximum-likelihood estimation was applied as a fallback. Selective pressure on duplicate pairs was inferred from the Ka/Ks ratio. Divergence time (T) between duplicated gene pairs was estimated using:

$T = Ks / (2 \times 6.5 \times 10^{-9}) \times 10^{-6}$

where 6.5×10^{-9} substitutions per site per year represents the assumed synonymous substitution rate for dicotyledonous plants. Divergence time was expressed in million years ago (MYA).

Phylogeny, gene structure, promoter analysis, and protein features

Full-length Car_Chit proteins were aligned using MUSCLE, and a neighbor-joining tree was reconstructed in MEGA X with 1000 bootstrap replicates [29]. Exon–intron structures were derived from genome annotation and visualized with GSDS 2.0 [30]. For promoter analysis, 1.5-kb upstream sequences were scanned in PlantCARE for ten preselected cis-elements associated with hormone responsiveness, defense/stress signaling, and light responsiveness [31]. Protein molecular weight and theoretical pI were calculated with ExPASy [32], signal peptides were predicted with SignalP 6.0 [33], subcellular localization was predicted with DeepLoc 2.0 [34], and conserved motifs were identified with MEME using a motif width range of 4–50 residues [35].

Candidate selection from public simulated-herbivory RNA-seq data

A public chickpea RNA-seq dataset generated under simulated herbivory (NCBI SRA accession SRP078184) [16] was used only as a discovery resource to prioritize candidate genes for field validation. Eleven Car_Chits (Car_Chit-3, -4, -11, -12, -13, -14, -17, -19, -20, -27, and -28) were selected for downstream qRT-PCR analysis because they exhibited differential expression in that dataset. No new whole-transcriptome sequencing was generated in the present study, and the public RNA-seq data were not used to infer de novo field regulatory networks.

Plant materials, treatments, and field sampling

Field experiments were conducted at the research farm of the ICAR–Indian Institute of Pulses Research, Kanpur, India (26°28′N, 80°20′E), using the chickpea cultivar ICC86111. Four treatments were evaluated: untreated control, *H. armigera* infestation, jasmonic acid (JA; 0.5 mM) foliar spray, and salicylic acid (SA; 200 µM) foliar spray. Treatments were arranged in three replicate blocks, with 20 plants per treatment in each block. At the flowering stage (82 days after sowing), plants assigned to herbivory were infested with five laboratory-reared third-instar *H. armigera* larvae per plant following 3–4 h pre-starvation. JA and SA were applied as foliar sprays to saturation.

Leaf tissue from the third to fifth positions was sampled at 0, 0.5, 1, 2, 4, 8, 24, and 48 h after treatment. Sampling was destructive: each plant was harvested once, and no plant contributed material to more than one time point. For each treatment × time combination, three independent biological replicates were collected. Tissues were briefly washed, cut into small pieces, immersed in RNAlater, and stored for RNA isolation.

RNA extraction and qRT-PCR analysis

Total RNA was extracted from 100 mg of leaf tissue for each biological replicate. First-strand cDNA was synthesized from 2 µg of RNA using the High-Capacity cDNA Reverse Transcription Kit (Applied Biosystems). qRT-PCR was performed with SYBR Green qPCR Master Mix (Agilent), using actin as the reference gene. Gene-specific primers for the eleven selected *Car_Chits* are listed in Additional file 1. Reactions were run in 384-well plates with an initial denaturation at 95 °C for 1 min, followed by 40 cycles of 95 °C for 15 s and 58–61 °C for 30 s. Relative expression was calculated using the 2^−ΔΔCt method with the untreated 0 h control as the calibrator. Statistical analyses were performed on $\log_2$FC

(−ΔΔCt) values from the biological replicates. Raw Ct values and derived expression data for Figure 3 are provided in Additional file 2.

Homology modelling and molecular docking

Seven Car_Chits (Car_Chit-4, -11, -14, -17, -19, -20, and -27) were selected for structural comparison. Protein sequences were retrieved from NCBI, and homologous templates were identified by BLAST searches against the Protein Data Bank. Template suitability was assessed using E-value, sequence identity, alignment coverage across the catalytic domain, and conservation of catalytic or active-site residues. Where multiple templates were available, the template with the best combination of catalytic-domain coverage, sequence identity, and active-site conservation was selected for modelling; as a practical reliability guide, retained models required broad catalytic-domain coverage and approximately 30% or higher sequence identity, or unambiguous conservation of the chitinase fold and active-site architecture when sequence identity was lower. Car_Chit-3 was not modelled because available PDB hits did not provide a suitable full catalytic-domain template meeting these quality criteria. Homology models were constructed with MODELLER v9.12 [36], and model quality was assessed using PROCHECK Ramachandran plots [37].

Docking against the chitin tetramer N-acetylglucosamine tetrasaccharide $(GlcNAc)_4$ was performed in AutoDock 4.2 via AutoDock Tools [38]. Ligand coordinates were obtained from crystal structures 1KR0 (GH18) and 3WH1 (GH19), and active sites were defined according to prior chitinase structural analyses [39]. Docked complexes were inspected in PyMOL and used as starting structures for molecular dynamics simulations. The $(GlcNAc)_4$ ligand was used as a standardized comparative substrate for relative prioritization; it was not intended to represent the full physical complexity of fungal cell-wall chitin, polymeric chitin, or the insect peritrophic matrix.

Molecular dynamics simulations and MM-PBSA calculations

Molecular dynamics simulations were performed in GROMACS v2020.4 [40] for 100 ns in explicit solvent. Protein systems were described using the CHARMM36 all-atom additive protein force field [41], and compatible ligand parameters were applied for $(GlcNAc)_4$. Trajectories were saved every 10 ps and analyzed for backbone RMSD, ligand RMSD, RMSF, radius of gyration (Rg), protein–ligand hydrogen bonds, and ligand–receptor center-of-mass (COM) distance. The first 10 ns were treated as equilibration, and summary statistics are reported for the 10–100 ns production interval. Hydrogen-bond traces were binned for visualization purposes only.

Binding free energies were estimated every 1 ns using the g_mmpbsa implementation of MM-PBSA [42], following the single-trajectory framework described by Genheden and Ryde [43]. ΔG_bind values are reported as mean ± SD over the 10–100 ns production window. Docking, MD, and MM-PBSA outputs were interpreted as comparative indicators of predicted ligand recognition and complex stability, not as direct measurements of catalytic activity, substrate turnover, or in planta defence function.

Statistical analysis

For each gene, $\log_2$FC values were analyzed using factorial linear models that included treatment, time, and the treatment × time interaction. Field blocks were incorporated during experimental layout to reduce spatial heterogeneity, and inferential testing was performed on the independent biological replicates

obtained at each treatment × time cell. For each gene-wise model, F statistics, nominal P values, and Benjamini–Hochberg false discovery rate (FDR)–adjusted q values were computed across the 11 profiled genes. Time-specific treatment responses were further evaluated with two-sided one-sample tests of $\log_2FC = 0$, and multiplicity for these contrasts was controlled within each gene across all treatment × time comparisons using BH-FDR. Differences with $q < 0.05$ were considered statistically significant. Asterisks in Figure 3 denote time-specific treatment responses with BH-FDR-adjusted $q < 0.05$ and do not denote nominal P values.

Results

Genome-wide identification of Car_Chit loci

Domain-based screening identified 28 chickpea chitinase loci distributed across the eight chromosomes (Table 1). The updated RefSeq annotation resolved 28 loci, including chromosomal placement of two genes that were previously unplaced or scaffold-associated (now *Car_Chit-16* on Ca4 and *Car_Chit-18* on Ca5). The loci were designated *Car_Chit-1* to *Car_Chit-28* according to chromosome order and genomic position. Six loci (21.4%; *Car_Chit-3, -4, -11, -12, -20*, and -24) belonged to the GH19 family, whereas the remaining 22 loci (78.6%) belonged to GH18. Protein lengths ranged from 237 aa (Car_Chit-21) to 769 aa (Car_Chit-22), highlighting marked structural diversity within the family. Predicted proteins also varied widely in molecular weight, theoretical pI, and signal peptide/localization features (Table 1).

Table 1. Detailed information about 28 predicted chickpea chitinase genes with protein accession, length (aa), theoretical pI, theoretical MW, and SignalP 6.0 / DeepLoc 2.0 annotations.

Gene	Locus / transcript	Chr	Coordinates (bp)	Strand	Exons	Protein accession	Length (aa)	Theoretical pI	Theoretical MW (Da)	SignalP-6.0 / DeepLoc-2.0	Family
Car_Chit-1	LOC101499824	Ca1	43497631-43498779	-	1	XP_004488666	303	5.31	34195.37	Other (Cytoplasm, Extracellular)	GH18
Car_Chit-2	LOC101507126	Ca1	46041184-46042183	-	1	XP_004487751	303	4.95	34635.98	Other (Cytoplasm)	GH18
Car_Chit-3	LOC101495915	Ca1	52278259-52283448	-	3	XP_027187340	272	5.86	30160.58	SP (Extracellular)	GH19
Car_Chit-4	LOC105851081	Ca1	52285894-52287392	-	2	XP_012570981	274	4.74	29832.12	SP (Extracellular)	GH19
Car_Chit-5	LOC101496480	Ca2	65906647-65914774	+	1	XP_004489751	275	5.03	31860.34	Other (Cytoplasm)	GH18
Car_Chit-6	LOC11378547	Ca	65974716-	+	1	XP_027187842	262	5.43	30461.96	Other (Cytoplasm,	GH18

	5	2	6598204			7				Nucleus)	
Car_Chit-7	LOC101497138	Ca2	6607461-66082028	+	1	XP_004489753	255	5.06	29478.91	Other (Cytoplasm, Nucleus)	GH18
Car_Chit-8	LOC101497470	Ca2	6625576-66626403	+	1	XP_004489754	275	5.54	32157.86	Other (Cytoplasm)	GH18
Car_Chit-9	LOC101508922	Ca2	6658631-66659458	+	1	XP_012568248	275	5.54	32157.86	Other (Cytoplasm)	GH18
Car_Chit-10	LOC101495610	Ca2	11486210-11487511	-	1	XP_004490140	294	7.51	31551.72	SP (Extracellular)	GH18
Car_Chit-11	LOC101492276	Ca3	17006532-17010471	-	3	XP_004492044	321	5.97	35734.39	SP (Extracellular)	GH19
Car_Chit-12	LOC101489718	Ca3	73927813-73929651	+	2	XP_004494478	278	7.5	31060.39	SP (Extracellular)	GH19
Car_Chit-13	LOC101502863	Ca4	11686179-11687236	+	1	NP_001296619	293	4.7	31229.81	SP (Extracellular)	GH18
Car_Chit-14	LOC101503186	Ca4	11690572-11691774	+	1	XP_004496498	298	9.03	32369.85	SP (Extracellular)	GH18
Car_Chit-15	LOC101503505	Ca4	11693847-11694900	+	1	XP_004496499	294	7.6	32399.73	SP (Extracellular)	GH18
Car_Chit-16	LOC101512927	Ca4	34622373-34623636	-	1	XP_004514594	309	5.37	34368.29	SP (Extracellular, Lysosome/Vacuole)	GH18
Car_Chit-17	LOC101499789	Ca4	60546842-60549104	+	2	XP_004498784	377	8.29	42524.08	SP (Extracellular)	GH18
Car_Chit-18	LOC101505007	Ca5	4345095-4346143	+	1	XP_004515450	300	8.97	32838.25	SP (Extracellular)	GH18
Car_Chit-19	LOC101501606	Ca5	76011861-76013511	-	2	XP_004501097	363	7.72	39283.91	SP (Extracellular)	GH18

Car_Chit-20	LOC101513497	Ca5	79126816-79128139	-	1	NP_001265906	328	7.37	35472.85	SP (Extracellular)	GH19
Car_Chit-21	LOC101515026	Ca6	27587037-27594991	+	1	XP_004503412	237	5.2	27470.86	Other (Cytoplasm)	GH18
Car_Chit-22	LOC101500690	Ca7	5731423-5735635	+	8	XP_004508381 XP_007322704 XP_012573472	769 767 740	7.57 7.57 7.56	87192.45 87034.29 83903.65	SP (Cell membrane) SP (Cell membrane) SP (Cell membrane)	GH18
Car_Chit-23	LOC101501002	Ca7	5737099-57403398	+	2	XP_004508382	382	5.77	41672.43	SP (Extracellular)	GH18
Car_Chit-24	LOC101511073	Ca7	16774912-16778501	-	3	XP_004509418	318	5.96	34399.26	SP (Extracellular)	GH19
Car_Chit-25	LOC101498991	Ca7	17441196-17442029	+	1	XP_004509468	277	5.65	32257.67	Other (Cytoplasm)	GH18
Car_Chit-26	LOC101513860	Ca7	26434122-26435487	+	2	XP_004511217	297	8.1	32639.45	SP (Extracellular)	GH18
Car_Chit-27	LOC101512905	Ca7	26512927-26514029	+	1	XP_004511214	296	4.97	31307.22	SP (Extracellular, Lysosome/Vacuole)	GH18
Car_Chit-28	LOC101513757	Ca8	7126826-7131696	+	8	XP_004512315	433	8.72	49219.91	Other (Endoplasmic reticulum)	GH18

Local duplication predominantly expanded GH18 members

The 28 *Car_Chits* were distributed across all eight chickpea chromosomes, with Ca2 and Ca7 each harboring six loci and Ca4 harboring five (Figure 1). Duplication analysis identified 15 dispersed genes, 10 tandem genes, 2 proximal genes, and 1 singleton, whereas no locus was classified as WGD/segmental. Tandem duplicates formed a five-gene array on Ca2 (*Car_Chit-5* to *Car_Chit-9*), a three-gene array on Ca4 (*Car_Chit-13* to *Car_Chit-15*), and a tandem pair on Ca7 (*Car_Chit-22* and *Car_Chit-23*). The proximal pair *Car_Chit-26/Car_Chit-27* was also confined to GH18. The Ca7 *Car_Chit-22/Car_Chit-23* tandem pair represents an additional local duplication resolved in the updated assembly relative to the

earlier 27-gene inventory [17]. These patterns indicate that local small-scale duplication, rather than large-scale segmental duplication, was the dominant driver of chitinase family expansion in chickpea.

All interpretable non-identical duplicate pairs showed Ka/Ks ratios below 1, ranging from 0.0368 to 0.5455, consistent with predominant purifying selection (Additional file 3). *Car_Chit-8* and *Car_Chit-9* encoded identical predicted proteins, producing Ka = 0 and Ks = 0; accordingly, Ka/Ks was undefined for that pair rather than zero. The exceptionally high Ks estimate for *Car_Chit-22/Car_Chit-23* suggests synonymous-site saturation and should be interpreted cautiously, even though the pair also falls below the neutrality threshold.

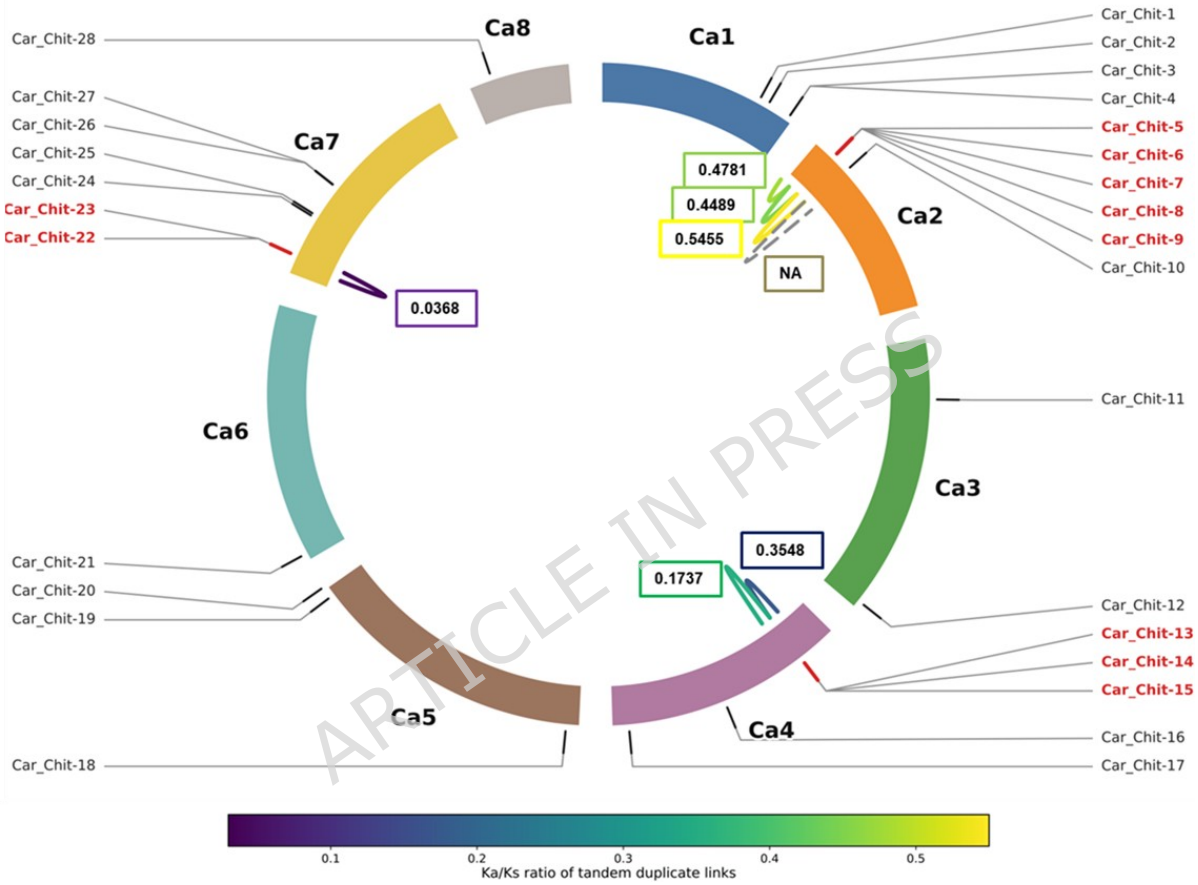

Figure 1. Circos plot showing the chromosomal distribution, tandem duplication events, and Ka/Ks ratios of the Car_Chit gene family in chickpea. The dashed grey link denotes the Car_Chit-8/Car_Chit-9 pair, for which Ka/Ks is undefined because the CDS sequences are identical (Ka = 0, Ks = 0).

Divergence time estimation of duplicated gene pairs

Divergence time analysis indicated that most interpretable duplication events occurred within approximately 1.3 to 11.9 million years ago (MYA), based on Ks-derived estimates. For example, the Car_Chit-7/8 pair showed the most recent duplication (~1.28 MYA), whereas Car_Chit-13/14 represented an older duplication event (~11.93 MYA). In contrast, the Car_Chit-22/23 pair exhibited an estimated divergence time exceeding 140 MYA. Because this estimate is associated with a very high Ks value and predates the genus Cicer, it should not be treated as a precise duplication date; rather, it indicates a highly divergent retained pair for which synonymous-site saturation is likely.

Phylogeny, gene architecture, promoter composition, and protein motifs

Neighbor-joining analysis of the 27 non-redundant proteins separated GH19 and GH18 sequences into the expected major clades (Figure 2). GH19 genes grouped into classes I, II, and IV, whereas GH18 members occupied classes III and V. Car_Chit-17, -19, -22, and -23 formed a distinct class V clade. Gene structure organization was largely consistent with phylogenetic groupings: most class III GH18 loci were intronless; GH19 loci were generally intron-containing; and class V members showed two main architectures, with two-exon loci represented by Car_Chit-17, Car_Chit-19, and Car_Chit-23, and the highly expanded Car_Chit-22 locus containing eight exons. Car_Chit-28 was also structurally complex, with eight exons.

Promoter scans detected 106 selected cis-element matches across the 28 upstream regions (Additional files 4 and 5). Defense- and stress-related motifs were slightly more abundant than hormone-related motifs, with W-box and MYC-like elements being especially frequent. Car_Chit-25 and Car_Chit-12 contained the highest densities of the scanned motifs, whereas Car_Chit-3, -18, and -21 lacked all selected motifs in this exact-match screen. Several promoters contained ambiguous N stretches, indicating that those counts should be interpreted as minimum estimates. MEME analysis identified ten conserved motifs whose distributions broadly tracked phylogenetic relationships, supporting lineage-specific conservation of domain architecture (Additional file 6).

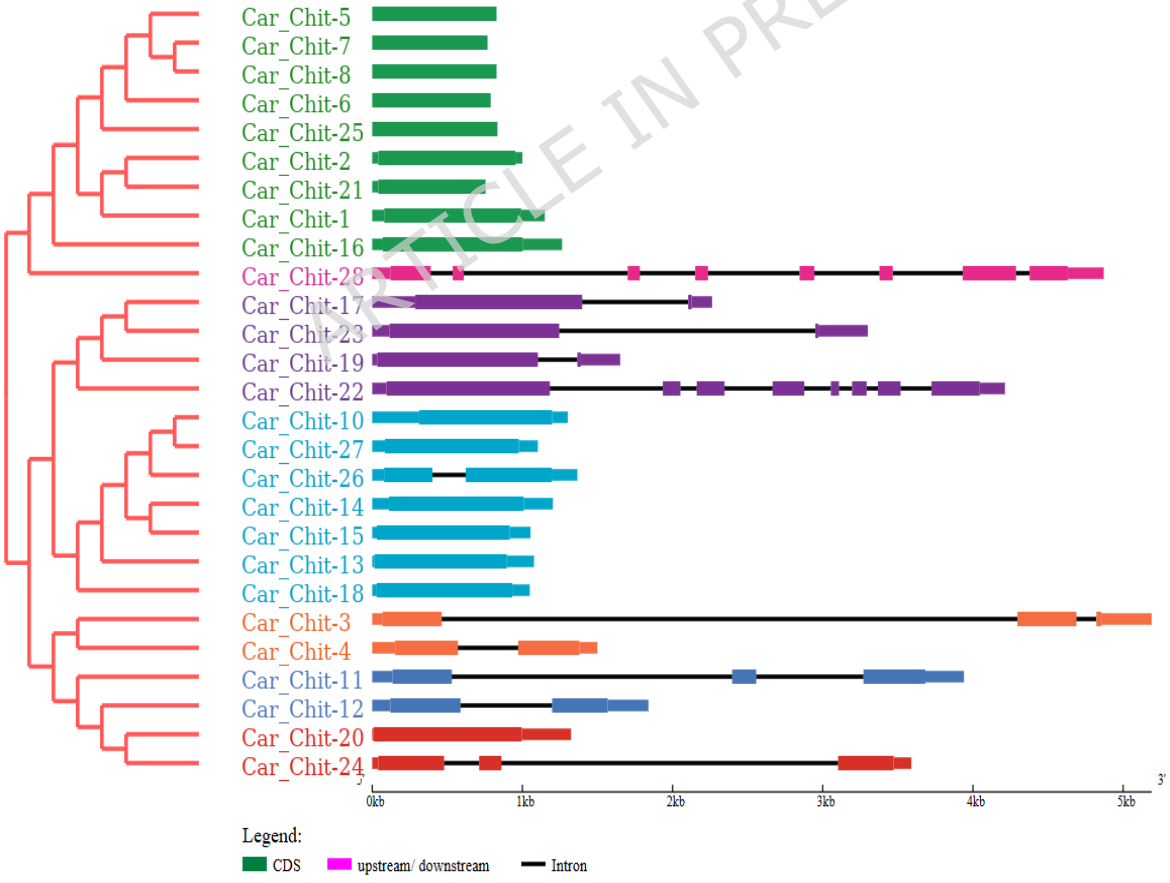

Figure 2. Integrated phylogenetic and gene-structure analysis of the Car_Chit family using the 27 non-redundant protein set. The left panel shows the neighbour-joining phylogeny reconstructed from full-length Car_Chit proteins with 1000 bootstrap replicates. The right panel shows exon-intron organization aligned to the same gene order; class V GH18 members include two-exon genes (Car_Chit-17, Car_Chit-19, and Car_Chit-23) and the eight-exon Car_Chit-22.

Field expression profiling reveals distinct herbivory and hormone responses

The simulated-herbivory RNA-seq dataset was used to select 11 Car_Chits for targeted field validation. In field-grown plants subjected to controlled *H. armigera* feeding, JA treatment, or SA treatment, qRT-PCR revealed strongly treatment- and time-dependent transcriptional behaviour (Figure 3). Relative expression is reported as fold change relative to the untreated 0 h control, and significance was assessed after BH-FDR correction. Because this experiment profiled selected chitinase genes rather than the whole transcriptome, the analysis was used to resolve time-dependent Car_Chit responses and not to infer genome-wide regulatory networks.

Under *H. armigera* infestation, *Car_Chit-19* was the clearest inducible GH18 gene, with significant up-regulation at 8 h (1.62-fold, $q = 0.050$) and 48 h (1.85-fold, $q = 0.050$). In contrast, *Car_Chit-4* showed marked early repression at 0.5 h (0.15-fold, $q = 0.030$). At 24 h, both *Car_Chit-14* (0.32-fold, $q = 0.045$) and *Car_Chit-19* (0.50-fold, $q = 0.050$) were significantly below the calibrator level, indicating a dynamic rather than monotonic response profile.

JA triggered broad early repression across several genes, including *Car_Chit-3, -11, -14, -17, -19, -27,* and *-28*, but *Car_Chit-4* showed delayed induction at 24 h (1.88-fold, $q = 0.047$). SA elicited the strongest response observed in the time course, with rapid induction of *Car_Chit-4* at 0.5 h (7.81-fold, $q = 0.026$) and 4 h (5.29-fold, $q < 0.05$). In contrast, several GH18 genes and *Car_Chit-3* were suppressed under SA, including *Car_Chit-14, -17, -19,* and *-27* at selected early or intermediate time points.

Taken together, the field expression data support differentiated temporal deployment of chickpea chitinases: Car_Chit-4 behaves as a rapid hormone-responsive GH19 gene, particularly under SA treatment, whereas Car_Chit-19 emerges as the clearest delayed herbivory-responsive GH18 candidate. The early repression of several genes under herbivory or JA treatment indicates that chitinase regulation is not monotonic and may involve transient suppression, pathway crosstalk, or phase-specific defence allocation before later induction of selected family members.

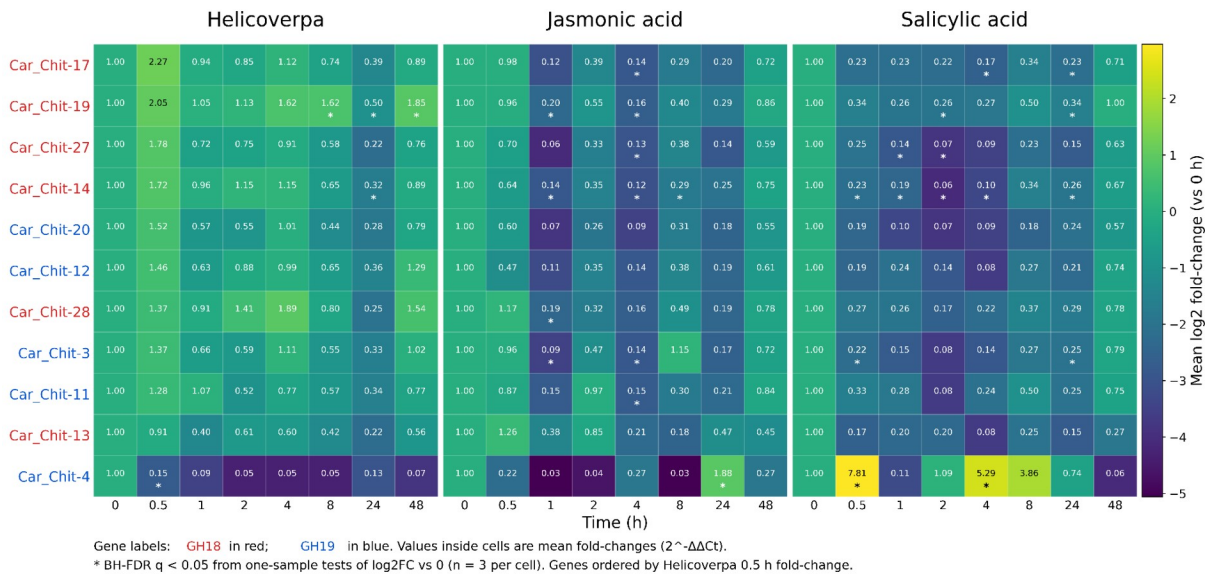

Figure 3. Side-by-side heatmaps showing Car_Chit expression over time in response to Helicoverpa infestation, jasmonic acid, and salicylic acid. Colour encodes mean $log_2(2^{-\Delta\Delta Ct})$ relative to the 0 h control; numbers inside cells are fold changes. Asterisks denote time-specific treatment responses with BH-FDR-adjusted $q < 0.05$ ($n = 3$ independent biological replicates per treatment × time cell).

Structure-guided comparison provides complementary biochemical prioritization

Homology modelling generated comparative structural models for selected Car_Chit proteins. PROCHECK Ramachandran plots and summary validation statistics supported the suitability of these models for relative, structure-guided comparisons (Additional files 7 and 8).

Among the models, Car_Chit-19 exhibited the highest structural quality, with 94.2% of residues in the most favored regions and no residues in disallowed regions, indicating excellent backbone geometry. Other models such as Car_Chit-4, -14, and -20 also showed strong stereochemical quality (>90% favored regions). Although a few models (Car_Chit-11, -17, and -27) exhibited slightly lower favored region percentages (~88–90%), their overall quality remained within acceptable limits, supporting their use in downstream analyses.

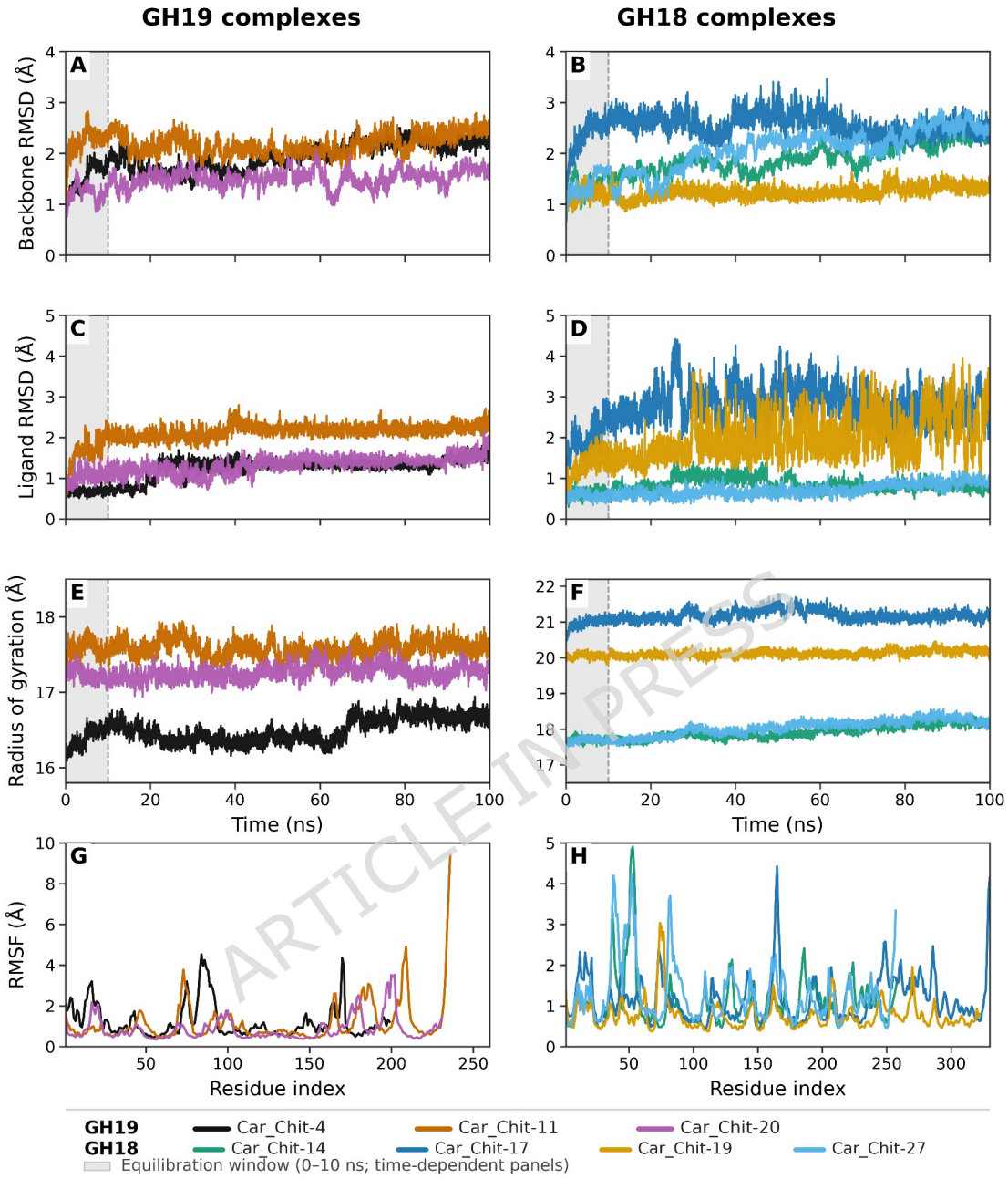

Figure 4. Time-resolved molecular dynamics analysis of Car_Chit-$(GlcNAc)_4$ complexes over 100 ns. Panels show backbone RMSD, ligand RMSD, radius of gyration, and residue-wise RMSF. The shaded region denotes the 0-10 ns equilibration interval.

Docking analysis produced plausible Car_Chit-$(GlcNAc)_4$ complexes for all selected proteins. The ligand was accommodated within predicted catalytic clefts, forming hydrogen bonds and hydrophobic contacts with conserved active-site or cleft-associated residues. These docking poses were used as starting conformations for simulation and should be interpreted as comparative models rather than proof of natural substrate binding or catalytic activity. Among GH19 proteins, Car_Chit-4 showed the most favourable docking score (−4.2 kcal/mol), whereas among GH18 proteins Car_Chit-19 showed the most favourable

docking score (−7.4 kcal/mol) (Additional file 9). These docked complexes were subsequently subjected to 100 ns molecular dynamics simulations.

Across the production interval, all complexes retained overall structural stability, but protein and ligand behavior differed among family members (Figures 4 and 5; Additional file 10). *Car_Chit-19* displayed the most stable GH18 protein scaffold, with the lowest backbone RMSD (1.24 ± 0.11 Å) and lowest average RMSF (0.77 ± 0.36 Å). *Car_Chit-14* and *Car_Chit-27* showed the strongest ligand-pose retention, each maintaining sub-Å ligand RMSD values. Within GH19, *Car_Chit-4* and *Car_Chit-20* retained the ligand more consistently than *Car_Chit-11*, which exhibited high COM separation and weak hydrogen-bond persistence despite a relatively favorable mean binding energy.

MM-PBSA comparisons further differentiated the candidate set. Because GH18 and GH19 chitinases differ in fold, catalytic architecture, and substrate-binding cleft organization, direct cross-family comparisons of predicted binding energies were interpreted cautiously. Within the standardized tetramer-binding comparison, GH18 proteins exhibited more favourable mean predicted binding energies than GH19 proteins overall. Car_Chit-17 produced the most favourable ΔG_bind (−18.51 ± 6.75 kcal/mol), followed by Car_Chit-14 (−13.93 ± 6.43 kcal/mol). Car_Chit-19 and Car_Chit-27 also showed negative binding energies consistent with stable predicted interaction. These analyses provide a structure-guided prioritization that complements, rather than replaces, the expression results.

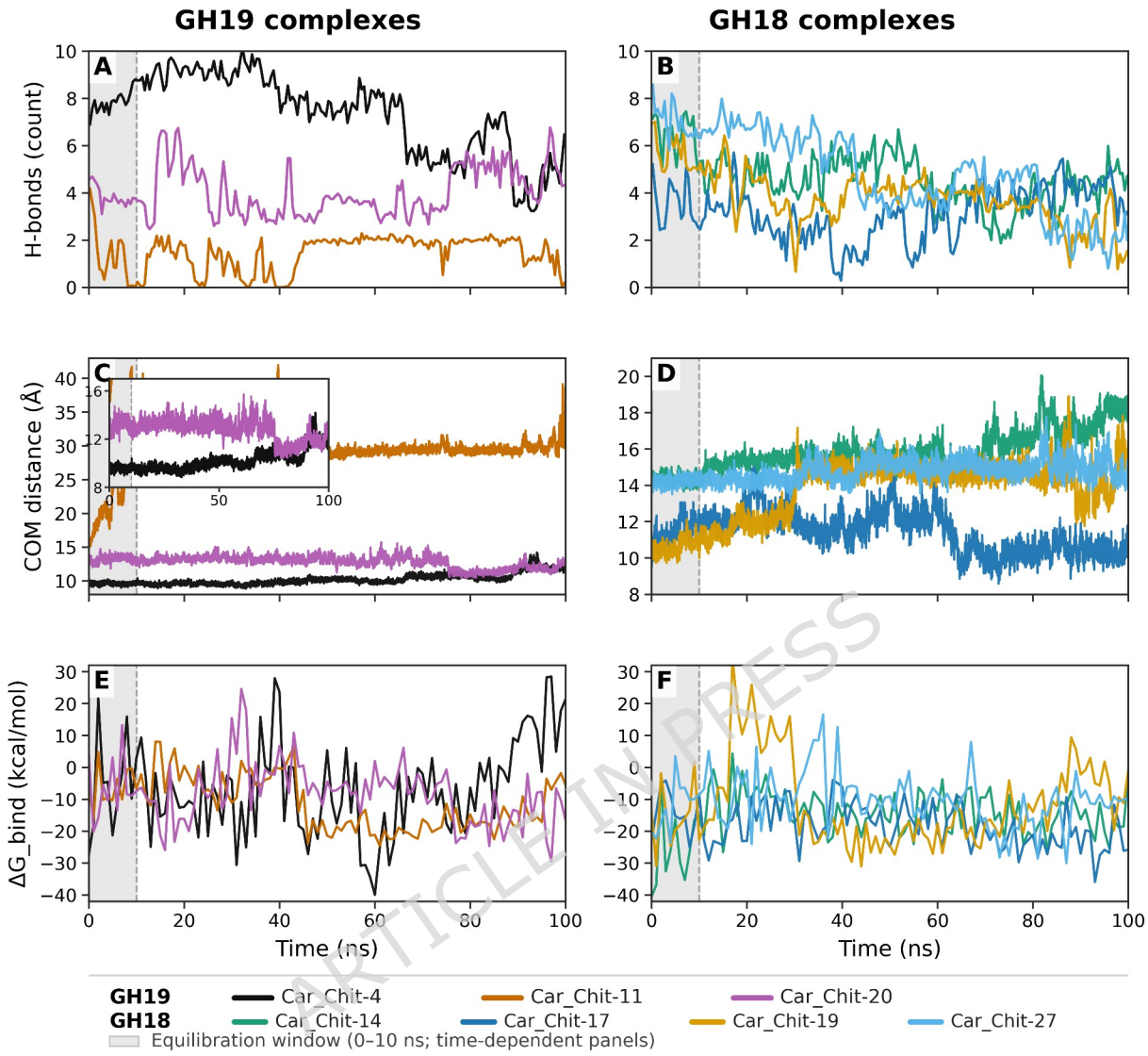

Figure 5. Time-resolved analysis of interaction stability and binding energetics of Car_Chit-(GlcNAc)4 complexes over 100 ns. Panels show protein-ligand hydrogen bonds, centre-of-mass distance, and MM-PBSA binding free energy. More negative ΔG_bind values indicate stronger predicted binding.

Table 2. Evidence-based prioritization framework linking genomic, expression, and structural evidence for selected Car_Chit candidates.

Evidence category	Candidate(s)	Interpretation and next validation step
Rapid hormone-responsive candidate	Car_Chit-4 (GH19)	Strong early SA induction and delayed JA induction, but transient early repression under *H. armigera*. Prioritized for in planta hormone-response and herbivory-validation assays.
Delayed herbivory-responsive candidate	Car_Chit-19 (GH18)	Most consistent late induction under *H. armigera* and most stable protein scaffold in MD. Prioritized for in planta validation and enzyme assays.
Structure-guided biochemical candidates	Car_Chit-17, Car_Chit-14, Car_Chit-27 (GH18)	Favourable predicted ΔG_bind or ligand-pose retention in the standardized $(GlcNAc)_4$ comparison. Prioritized for recombinant expression, kinetic assays, and substrate-length testing.
Genomic expansion background	GH18 tandem/proximal duplicates	Local duplication expanded the family under purifying selection. Prioritized for comparative promoter, expression, and functional-divergence analyses.

Discussion

The present study investigated whether Helicoverpa herbivory induces chickpea chitinase gene expression and whether the induced chitinases differ in their capacity to recognize a common chitin ligand. We demonstrate that GH18 and GH19 Car_Chits display distinct expression patterns under field herbivory and phytohormone treatments, and that their predicted $(GlcNAc)_4$ recognition and complex stability differ in silico, with GH18 members generally exhibiting more favourable tetramer-binding metrics than GH19. The results are best interpreted through a tiered framework: genome analysis identifies the family structure and duplication history, field qRT-PCR identifies transcriptionally deployed candidates, and structural modelling prioritizes candidates for enzyme-level biochemical testing.

Chickpea chitinases expanded mainly through local GH18 duplication and were retained under purifying selection

We identified 28 chickpea chitinase loci, of which 22 belong to GH18 and 6 to GH19. A recent chickpea study focused on *Fusarium* stress reported 27 chitinase genes [17]; compared with that assembly-based inventory, our updated RefSeq analysis supports 28 loci, anchors two formerly unplaced genes to Ca4 and Ca5, and resolves an additional tandem duplicate on Ca7. In a broader comparative context, the chickpea family size is comparable to *Arabidopsis* (24 genes) but lower than in pigeonpea (34 genes) and soybean (35 genes) [9, 44–45]. The most distinctive feature of the chickpea family was not simply the numerical predominance of GH18 members but the duplication pattern: tandem and proximal duplications were confined to GH18, whereas GH19 loci remained more dispersed. Together with the absence of detectable WGD or segmental duplicates, this pattern indicates that local duplication and retention were the primary drivers of family expansion.

The consistently low Ka/Ks ratios across interpretable duplicate pairs indicate that most retained copies evolved under purifying selection, preserving core catalytic and structural properties after duplication. At the same time, the relatively recent divergence times estimated for most pairs suggest that tandem duplication has remained an active mechanism for expanding the family, whereas the highly divergent Car_Chit-22/23 pair represents an older retained duplication whose Ks value is likely affected by synonymous-site saturation. These patterns are more consistent with regulatory diversification than with rapid coding-sequence neofunctionalization, an interpretation supported by differences in promoter motif composition and inducible expression among related loci.

Expression data support temporally distinct GH19 and GH18 response modules

The field expression experiment distinguishes this study from earlier chickpea work based on simulated herbivory [16]. Under controlled insect feeding, the strongest transcriptional responses were not a broad up-regulation of the profiled family but rather an early repression of Car_Chit-4 and a delayed induction of Car_Chit-19. This divergence from simulated-herbivory transcriptomes is biologically plausible, as chewing insects deliver oral secretions, gut-derived elicitors, associated microbes, and complex tissue-damage cues that are not fully recapitulated by mechanical injury [20-22, 46-47]. Such herbivore-associated signals can either activate or attenuate particular defence branches, making transient repression of selected chitinases compatible with an active and temporally structured defence response.

The hormone time courses reinforce this interpretation. Car_Chit-4 showed strong responsiveness to SA and modest late induction by JA, whereas Car_Chit-19 was the only profiled gene with clear late induction under *H. armigera* feeding. This pattern supports a working model of two temporally distinct response modules rather than a unified chitinase program: a rapid, GH19-associated SA-responsive arm exemplified by Car_Chit-4, and a later, GH18-associated herbivory-responsive arm exemplified by Car_Chit-19. The broader early repression under JA and the absence of simple co-induction by SA and herbivory are consistent with known antagonistic or context-dependent interactions among defence pathways [48-52]. Therefore, repression at early time points should not be interpreted as lack of chitinase involvement, but as evidence that timing and hormonal context are central to chitinase deployment.

Structural analyses prioritize biochemical candidates

The docking, molecular dynamics, and MM-PBSA analyses add a biochemical dimension to the study by distinguishing transcriptional candidates from ligand-recognition candidates. GH18 members generally exhibited more favourable predicted $(GlcNAc)_4$ interaction energetics than GH19 members under the standardized simulation setup, yet the structural analyses revealed that affinity, pose retention, and scaffold stability are not interchangeable metrics. Car_Chit-17 showed the most favourable mean ΔG_bind, Car_Chit-14 and Car_Chit-27 best retained the ligand pose, and Car_Chit-19 provided the most stable protein scaffold. This explains why the structural ranking does not perfectly match the field-expression ranking: expression identifies deployment under a treatment, whereas modelling estimates relative interaction behaviour toward one standardized chitin oligomer. These observations should be viewed as comparative prioritization rather than definitive evidence of anti-herbivore activity. The models were derived from homology templates, the simulations employed a single ligand class and one 100-ns trajectory per complex, and substrate recognition by GH19 enzymes may differ for longer oligomers owing to the broader and flexible binding cleft previously described for family 19 chitinases [53–55]. GH18 and GH19 chitinases also differ in fold and catalytic architecture, so tetramer binding metrics should not be used to infer cross-family catalytic superiority. Accordingly, the most defensible conclusion is that the structural analyses nominate Car_Chit-17, -14, and -27 for biochemical characterization, whereas the expression data nominate Car_Chit-19 and Car_Chit-4 for in planta validation.

Limitations and future directions

This study was conducted in a single chickpea genotype and one field environment, leaving genotype-by-environment effects unresolved. The qRT-PCR experiment employed three biological replicates per treatment × time point, sufficient to detect strong responses but with limited power for subtle transcriptional changes. Because no new field RNA-seq dataset was generated, the study cannot define transcriptome-wide differentially expressed genes, co-expression modules, or regulatory networks under *H. armigera*, JA, or SA treatments. In the computational analyses, homology models substituted for experimentally solved structures, and simulations focused on the chitin tetramer rather than a broader

panel of oligomers or polymeric substrates. Finally, expression and in silico ligand-recognition data nominate candidates but do not establish enzyme activity, anti-herbivore efficacy, or causal defence function.

Future work should therefore proceed in three directions: first, matched field RNA-seq across herbivory, JA, and SA treatments, multiple time points, genotypes, and environments to resolve regulatory networks; second, functional testing of prioritized genes through recombinant enzyme assays, substrate-specific kinetics, transient or stable overexpression, knockdown or genome-editing approaches, and herbivore performance assays; and third, expanded computational comparisons incorporating longer oligomers, replicate simulations, polymeric or peritrophic-matrix-relevant substrates, and substrate-length-specific biochemical measurements. These steps will be essential to determine whether the transcriptionally responsive genes and structurally prioritized genes converge on a common defence mechanism.

Conclusions

This study establishes a genome-wide framework for chickpea chitinases, linking genomic organization to field expression dynamics and structure-guided candidate prioritization. Chickpea harbours 28 Car_Chit loci, with family expansion driven primarily by local duplication within GH18. Expression profiling in field-grown plants under controlled *H. armigera* infestation and hormone treatments supports a model in which GH19 Car_Chit-4 defines a rapid SA-responsive arm, while GH18 Car_Chit-19 defines a delayed herbivory-responsive arm. Complementary docking and molecular dynamics analyses nominate Car_Chit-17, -14, and -27 as leading biochemical candidates. By separating expression-deployed candidates from structure-guided biochemical candidates, the framework provides a focused set of chitinase targets for functional validation in chickpea defence biology, while recognizing that direct anti-herbivore activity remains to be demonstrated experimentally.

List of abbreviations

Abbreviation	Definition
COM	centre of mass
DE	differentially expressed
FDR	false discovery rate
FC	fold change
GH	glycosyl hydrolase
JA	jasmonic acid
Ka	nonsynonymous substitution rate
Ks	synonymous substitution rate
MD	molecular dynamics
MM-PBSA	molecular mechanics/Poisson-Boltzmann surface area
PR	pathogenesis-related
qRT-PCR	quantitative real-time PCR
Rg	radius of gyration
RMSD	root mean square deviation
RMSF	root mean square fluctuation
SA	salicylic acid
SAR	systemic acquired resistance
SRA	Sequence Read Archive

WGD	whole-genome duplication

Declarations

Ethics approval and consent to participate

Chickpea plants used in this study were cultivated at the ICAR-Indian Institute of Pulses Research research farm and did not involve collection of wild or protected plant material. The insect work used laboratory-reared *Helicoverpa armigera*, an agricultural pest species. Under institutional practice for experiments involving cultivated plants and unregulated invertebrates, no specific ethics approval was required.

Consent for publication

Not applicable.

Availability of data and materials

The public RNA-seq dataset re-analysed in this study is available in the NCBI Sequence Read Archive under accession SRP078184. No new whole-transcriptome RNA-seq dataset was generated in this study. All other data generated or analysed during this study are included in this manuscript and its additional files. Raw qRT-PCR Ct values and derived expression calculations underlying Figure 3 are submitted as Additional file 2 (.xlsx).

Competing interests

The authors declare that they have no competing interests.

Funding

This work was supported by the institute-funded project CRSCIIPRSIL202000400159 and by the project funded by Anusandhan National Research Foundation (ANRF), formerly known as Science and Engineering Research Board (SERB) EEQ/2022/000603.

Authors' contributions

AKK and GPD conceived and designed the study. AKK and HA performed the computational analyses. SGK, AKK, and HA conducted the field experiments and sampling. PS, AKK, and KJG performed the qRT-PCR analyses. BB and AKK carried out the homology modelling and docking work. AKK, HH, and SM performed the molecular dynamics simulations. AKK drafted the manuscript. KJG, SM, and GPD revised the manuscript critically.

All authors read and approved the final manuscript.

Acknowledgements

The authors thank the Directors of ICAR-IIPR, NIPGR, and IIT Kanpur for providing facilities to conduct the work. During the preparation of this manuscript, the authors used ChatGPT (OpenAI) for improving language clarity, readability, and organization.

References

1. Haile, Fikru, Tim Nowatzki, and Nicolas Storer. Overview of pest status, potential risk, and management considerations of Helicoverpa armigera (Lepidoptera: Noctuidae) for US soybean production. J Integr Pest Manag 12, no. 1 (2021): 3. https://doi.org/10.1093/jipm/pmaa030.

2. Sharma, H. C., P. C. Stevenson, and C. L. L. Gowda. Heliothis/Helicoverpa management: Emerging trends and prospects for future research. Oxford & IBH Publishing Co. Pvt. Ltd.: New Delhi, India (2005): 453-461.
3. Patil, Somanagouda B., Aakash Goyal, Satish S. Chitgupekar, Shiv Kumar, and Mustapha El-Bouhssini. Sustainable management of chickpea pod borer. A review. Agron Sustain Dev 37, no. 3 (2017): 1-17. https://doi.org/10.1007/s13593-017-0428-8.
4. Tabashnik, Bruce E., and Yves Carrière. Surge in insect resistance to transgenic crops and prospects for sustainability. Nat Biotechnol 35, no. 10 (2017): 926-935. https://doi.org/10.1038/nbt.3974.
5. Han, Yang, Erin B. Taylor, and Dawn Luthe. Maize endochitinase expression in response to fall armyworm herbivory. J Chem Ecol 47 (2021): 689-706.
6. Osman, Gamal H., Shireen K. Assem, Rasha M. Alreedy, Doaa K. El-Ghareeb, Mahmoud A. Basry, Anshu Rastogi, and Hazem M. Kalaji. Development of insect resistant maize plants expressing a chitinase gene from the cotton leaf worm, Spodoptera littoralis. Sci Rep 5, no. 1 (2015): 18067. https://doi.org/10.1038/srep18067.
7. Wiwat, Chanpen, Saranya Thaithanun, Somsak Pantuwatana, and Amaret Bhumiratana. Toxicity of chitinase-producing Bacillus thuringiensis ssp. kurstaki HD-1 (G) toward Plutella xylostella. J Invertebr Pathol 76, no. 4 (2000): 270-277.
8. Henrissat, Bernard. A classification of glycosyl hydrolases based on amino acid sequence similarities. Biochem J 280, no. 2 (1991): 309-316.
9. Passarinho, Paul A., and Sacco C. de Vries. Arabidopsis chitinases: a genomic survey. Arabidopsis Book 1 (2002):1:e0023. https://doi.org/10.1199/tab.0023.
10. Corrado, Giandomenico, Stefania Arciello, Paolo Fanti, Luisa Fiandra, Antonio Garonna, Maria Cristina Digilio, Matteo Lorito, Barbara Giordana, Francesco Pennacchio, and Rosa Rao. The Chitinase A from the baculovirus AcMNPV enhances resistance to both fungi and herbivorous pests in tobacco. Transgenic Res 17 (2008): 557-571.
11. Kramer, Karl J., and Subbaratnam Muthukrishnan. Insect chitinases: molecular biology and potential use as biopesticides. Insect Biochem Mol Biol 27, no. 11 (1997): 887-900.
12. Navarro-González, Samantha Sarai, José Augusto Ramírez-Trujillo, Guadalupe Peña-Chora, Paul Gaytán, Abigail Roldán-Salgado, Gerardo Corzo, Laura Patricia Lina-García, Víctor Manuel Hernández-Velázquez, and Ramón Suárez-Rodríguez. Enhanced tolerance against a fungal pathogen and insect resistance in transgenic tobacco plants overexpressing an endochitinase gene from Serratia marcescens. Int J Mol Sci 20, no. 14 (2019): 3482. https://doi.org/10.3390/ijms20143482.
13. Gatehouse, Angharad MR, Gillian M. Davison, Christine A. Newell, Andrew Merryweather, William DO Hamilton, Elisabeth PJ Burgess, Robert JC Gilbert, and John A. Gatehouse. Transgenic potato plants with enhanced resistance to the tomato moth, Lacanobia oleracea: growth room trials. Mol Breed 3 (1997): 49-63.
14. Lawrence, Susan D., and Nicole G. Novak. Expression of poplar chitinase in tomato leads to inhibition of development in Colorado potato beetle. Biotechnol Lett 28 (2006): 593-599.
15. Rathinam, Maniraj, Sathish Kumar Marimuthu, Shaily Tyagi, Karthik Kesiraju, Lakshmi Prabha Alagiamanavalan, Uma Rao, and Rohini Sreevathsa. Characterization and in planta validation of a CHI4 chitinase from Cajanus platycarpus (Benth.) Maesen for its efficacy against pod borer, Helicoverpa armigera (Hübner). Pest Manag Sci 77, no. 5 (2021): 2337-2349.
16. Pandey, Saurabh Prakash, Shruti Srivastava, Ridhi Goel, Deepika Lakhwani, Priya Singh, Mehar Hasan Asif, and Aniruddha P. Sane. Simulated herbivory in chickpea causes rapid changes in defense

pathways and hormonal transcription networks of JA/ethylene/GA/auxin within minutes of wounding. Sci Rep 7, no. 1 (2017): 1-14. https://doi.org/10.1038/srep44729.

17. Irum, Samra, Mustafa Cilkiz, Noorah Al-Kubaisi, Mohamed S. Elshikh, and Rashid Iqbal. Genome-wide characterization and expression analysis of the chitinase gene family in chickpea (Cicer arietinum L.) for fungal stress resistance. Mol Biol Rep 52 (2025): 871. https://doi.org/10.1007/s11033-025-10937-x.
18. Rakwal, Randeep, Guangxiao Yang, and Setsuko Komatsu. Chitinase induced by jasmonic acid, methyl jasmonate, ethylene and protein phosphatase inhibitors in rice. Mol Biol Rep 31, no. 2 (2004): 113-119.
19. Kellmann, Jan-Wolfhard, Tatjana Kleinow, Kerstin Engelhardt, Christina Philipp, Dorothee Wegener, Jeff Schell, and Peter H. Schreier. Characterization of two class II chitinase genes from peanut and expression studies in transgenic tobacco plants. Plant Mol Biol 30 (1996): 351-358.
20. Halitschke, Rayko, Ursula Schittko, Georg Pohnert, Wilhelm Boland, and Ian T. Baldwin. Molecular interactions between the specialist herbivore Manduca sexta (Lepidoptera, Sphingidae) and its natural host Nicotiana attenuata. III. Fatty acid-amino acid conjugates in herbivore oral secretions are necessary and sufficient for herbivore-specific plant responses. Plant Physiol 125, no. 2 (2001): 711-717.
21. Lortzing, Tobias, Vivien Firtzlaff, Duy Nguyen, Ivo Rieu, Sandra Stelzer, Martina Schad, Jim Kallarackal, and Anke Steppuhn. Transcriptomic responses of Solanum dulcamara to natural and simulated herbivory. Mol Ecol Resour 17, no. 6 (2017): e196-e211.
22. Heidel-Fischer, Hanna M., Richard O. Musser, and Heiko Vogel. Plant transcriptomic responses to herbivory. Annual Plant Reviews online (2018): 155-196.
23. Boratyn, Grzegorz M., Alejandro A. Schäffer, Richa Agarwala, Stephen F. Altschul, David J. Lipman, and Thomas L. Madden. Domain enhanced lookup time accelerated BLAST. Biol Direct 7, no. 1 (2012): 12.
24. Huang, Ying, Beifang Niu, Ying Gao, Limin Fu, and Weizhong Li. CD-HIT Suite: a web server for clustering and comparing biological sequences. Bioinformatics 26, no. 5 (2010): 680-682.
25. Letunic, Ivica, and Peer Bork. 20 years of the SMART protein domain annotation resource. Nucleic Acids Res 46, no. D1 (2018): D493-D496. https://doi.org/10.1093/nar/gkx922.
26. El-Gebali, Sara, Jaina Mistry, Alex Bateman, Sean R. Eddy, Aurélien Luciani, Simon C. Potter, Matloob Qureshi et al. The Pfam protein families database in 2019. Nucleic Acids Res 47, no. D1 (2019): D427-D432. https://doi.org/10.1093/nar/gky995.
27. Krzywinski, Martin, Jacqueline Schein, Inanc Birol, Joseph Connors, Randy Gascoyne, Doug Horsman, Steven J. Jones, and Marco A. Marra. Circos: an information aesthetic for comparative genomics. Genome Res 19, no. 9 (2009): 1639-1645.
28. Wang, Yupeng, Haibao Tang, Jeremy D. DeBarry, Xu Tan, Jingping Li, Xiyin Wang, Tae-ho Lee et al. MCScanX: a toolkit for detection and evolutionary analysis of gene synteny and collinearity. Nucleic Acids Res 40, no. 7 (2012): e49-e49.
29. Kumar, Sudhir, Glen Stecher, Michael Li, Christina Knyaz, and Koichiro Tamura. MEGA X: molecular evolutionary genetics analysis across computing platforms. Mol Biol Evol 35, no. 6 (2018): 1547-1549.
30. Hu, Bo, Jinpu Jin, An-Yuan Guo, He Zhang, Jingchu Luo, and Ge Gao. GSDS 2.0: an upgraded gene feature visualization server. Bioinformatics 31, no. 8 (2015): 1296-1297.

31. Lescot, Magali, Patrice Déhais, Gert Thijs, Kathleen Marchal, Yves Moreau, Yves Van de Peer, Pierre Rouzé, and Stephane Rombauts. PlantCARE, a database of plant cis-acting regulatory elements and a portal to tools for in silico analysis of promoter sequences. Nucleic Acids Res 30, no. 1 (2002): 325-327.
32. Gasteiger, Elisabeth, Christine Hoogland, Alexandre Gattiker, S'everine Duvaud, Marc R. Wilkins, Ron D. Appel, and Amos Bairoch. Protein identification and analysis tools on the ExPASy server. Humana press, 2005.
33. Teufel, Felix, José Juan Almagro Armenteros, Alexander Rosenberg Johansen, Magnús Halldór Gíslason, Silas Irby Pihl, Konstantinos D. Tsirigos, Ole Winther, Søren Brunak, Gunnar von Heijne, and Henrik Nielsen. SignalP 6.0 predicts all five types of signal peptides using protein language models. Nature biotechnology 40, no. 7 (2022): 1023-1025.
34. Thumuluri, Vineet, José Juan Almagro Armenteros, Alexander Rosenberg Johansen, Henrik Nielsen, and Ole Winther. DeepLoc 2.0: multi-label subcellular localization prediction using protein language models. Nucleic Acids Res 50, no. W1 (2022): W228-W234.
35. Timothy L. Bailey and Charles Elkan,"Fitting a mixture model by expectation maximization to discover motifs in biopolymers", Proceedings of the Second International Conference on Intelligent Systems for Molecular Biology,(1994): 28-36.
36. Šali, Andrej. MODELER: a program for protein structure modeling release 9.12, r9480. Rockefeller Univ (2013): 779-815.
37. Laskowski, Roman A., Malcolm W. MacArthur, David S. Moss, and Janet M. Thornton. PROCHECK: a program to check the stereochemical quality of protein structures. J Appl Crystallogr 26, no. 2 (1993): 283-291.
38. Rizvi, Syed Mohd Danish, Shazi Shakil, and Mohd Haneef. A simple click by click protocol to perform docking: AutoDock 4.2 made it easy for non-bioinformaticians. EXCLI J 12 (2013): 831.
39. Bhuvanachandra, Bhoopal, Jogi Madhuprakash, and Appa Rao Podile. Active-site mutations improved the transglycosylation activity of Stenotrophomonas maltophilia chitinase A. Biochim Biophys Acta Proteins Proteom 1866, no. 3 (2018): 407-414.
40. Abraham, Mark James, Teemu Murtola, Roland Schulz, Szilárd Páll, Jeremy C. Smith, Berk Hess, and Erik Lindahl. GROMACS: High performance molecular simulations through multi-level parallelism from laptops to supercomputers. SoftwareX 1 (2015): 19-25.
41. Huang, Jing, and Alexander D. MacKerell Jr. CHARMM36 all-atom additive protein force field: Validation based on comparison to NMR data. J Comput Chem 34, no. 25 (2013): 2135-2145. https://doi.org/10.1002/jcc.23354.
42. Kumari, Rashmi, Rajendra Kumar, Open Source Drug Discovery Consortium, and Andrew Lynn. g_mmpbsa A GROMACS tool for high-throughput MM-PBSA calculations. J Chem Inf Model 54, no. 7 (2014): 1951-1962.
43. Genheden, Samuel, and Ulf Ryde. The MM/PBSA and MM/GBSA methods to estimate ligand-binding affinities. Expert Opin Drug Discov 10, no. 5 (2015): 449-461.
44. Mahato, Ajay Kumar, Ajay Kumar Sharm, and Nagendra Kumar Singh. Genome-wide characterization and expression patterns of chitinase genes in the pigeonpea ('Cajanus cajan'(L.) Millsp.) genome. Plant Omics 12, no. 2 (2019): 109-119.
45. Lv, Peiyun, Chunting Zhang, Ping Xie, Xinyu Yang, Mohamed A. El-Sheikh, Daniel Ingo Hefft, Parvaiz Ahmad, Tuanjie Zhao, and Javaid Akhter Bhat. Genome-Wide Identification and Expression

Analysis of the Chitinase Gene Family in Response to White Mold and Drought Stress in Soybean (Glycine max). Life (Basel) 12, no. 9 (2022): 1340. https://doi.org/10.3390/life12091340.
46. Ray, Swayamjit, Patrick CMS Alves, Imtiaz Ahmad, Iffa Gaffoor, Flor E. Acevedo, Michelle Peiffer, Shan Jin et al. Turnabout is fair play: herbivory-induced plant chitinases excreted in fall armyworm frass suppress herbivore defenses in maize. Plant Physiol 171, no. 1 (2016): 694-706.
47. Chung, Seung Ho, Cristina Rosa, Erin D. Scully, Michelle Peiffer, John F. Tooker, Kelli Hoover, Dawn S. Luthe, and Gary W. Felton. Herbivore exploits orally secreted bacteria to suppress plant defenses. Proc Natl Acad Sci U S A 110, no. 39 (2013): 15728-15733.
48. Pieterse, Corné MJ, Saskia CM Van Wees, Johan A. Van Pelt, Marga Knoester, Ramon Laan, Han Gerrits, Peter J. Weisbeek, en Leendert C. Van Loon. A novel signaling pathway controlling induced systemic resistance in Arabidopsis. Plant Cell 10, no. 9 (1998): 1571-1580.
49. McConn, Michele, Robert A. Creelman, Erin Bell, John E. Mullet, and John Browse. Jasmonate is essential for insect defense in Arabidopsis. Proc Natl Acad Sci U S A 94, no. 10 (1997): 5473-5477.
50. Zarate, Sonia I., Louisa A. Kempema, and Linda L. Walling. Silverleaf whitefly induces salicylic acid defenses and suppresses effectual jasmonic acid defenses. Plant Physiol 143, no. 2 (2007): 866-875.
51. Thomma, Bart PHJ, Kristel Eggermont, Iris AMA Penninckx, Brigitte Mauch-Mani, Ralph Vogelsang, Bruno PA Cammue, and Willem F. Broekaert. Separate jasmonate-dependent and salicylate-dependent defense-response pathways in Arabidopsis are essential for resistance to distinct microbial pathogens. Proc Natl Acad Sci U S A 95, no. 25 (1998): 15107-15111.
52. Thaler, Jennifer S., Parris T. Humphrey, and Noah K. Whiteman. Evolution of jasmonate and salicylate signal crosstalk. Trends Plant Sci 17, no. 5 (2012): 260-270.
53. Ubhayasekera, Wimal, Ce Mun Tang, Sharon WT Ho, Gunnar Berglund, Terese Bergfors, Mee-Len Chye, and Sherry L. Mowbray. Crystal structures of a family 19 chitinase from Brassica juncea show flexibility of binding cleft loops. FEBS J 274, no. 14 (2007): 3695-3703.
54. Ubhayasekera, Wimal. Structure and function of chitinases from glycoside hydrolase family 19. Polym Int 60, no. 6 (2011): 890-896.
55. Sasaki, Chiye, Yoshifumi Itoh, Hideki Takehara, Satoru Kuhara, and Tamo Fukamizo. Family 19 chitinase from rice (Oryza sativa L.): substrate-binding subsites demonstrated by kinetic and molecular modeling studies. Plant Mol Biol 52 (2003): 43-52.

Additional files

Additional file 1 (.pdf). Primer sequences used for qRT-PCR analysis of selected Car_Chit genes. Gene-specific primer sequences, expected product lengths, and melting temperatures for the 11 profiled genes.

Additional file 2 (.xlsx). Raw qRT-PCR Ct values and derived expression calculations for all biological replicates used in Figure 3.

Additional file 3 (.pdf). Evolutionary divergence and selection pressure among duplicated Car_Chit gene pairs in chickpea. Table reporting duplication type, Ka, Ks, Ka/Ks, estimation method, divergence time, and inferred selection pressure.

Additional file 4 (.pdf). Consensus cis-element landscape in the 1.5-kb upstream promoter regions of the 28 Car_Chit genes. Figure showing the promoter motif heatmap and family-level motif totals.

Additional file 5 (.pdf). Counts of selected cis-regulatory motifs in 1.5-kb upstream promoters of the chickpea Car_Chit genes. Table reporting motif counts per promoter, motif definitions, and notes on ambiguous bases.

Additional file 6 (.pdf). Conserved motif distribution among chitinase proteins. Figure showing the spatial arrangement of the 10 MEME motifs across the analysed chitinase proteins.

Additional file 7 (.pdf). Ramachandran plot validation of predicted Car_Chit protein models. Figure summarizing PROCHECK Ramachandran plots for the selected homology models.

Additional file 8 (.pdf). Structural validation statistics and template-selection information of Car_Chit protein models. Table summarizing template identity/coverage information, residues in favoured/allowed regions, disallowed residues, and model-quality calls.

Additional file 9 (.pdf). Docking scores of selected Car_Chit proteins against (GlcNAc)4. Table reporting docking energies for the GH18 and GH19 representatives.

Additional file 10 (.pdf). Molecular dynamics-derived stability metrics and MM-PBSA binding energetics of Car_Chit-(GlcNAc)4 complexes. Table reporting RMSD, ligand RMSD, radius of gyration, RMSF, hydrogen bonds, centre-of-mass distance, and ΔG_bind over the production interval.